RESEARCH PAPER

Effect of Aging Duration on Mineral Composition, Microstructure, and Texture in a Malachite-based Co-precipitate and its Composite (Metallic)-Oxidic Derivatives

Mohammad H. Ghayour Anarjan[1], Maryam Mirasgari[2], Hajar Ghanbari[1,*], Hossein Sarpoolaky[1], Amin Mardanloo[2]

* *hajar_ghanbari@iust.ac.ir*

[1] School of Metallurgy and Materials Engineering, Iran University of Science & Technology, Narmak, Tehran, Iran
[2] Khwarizmi Technology Development Company, Garmdareh, Alborz, Iran

Received: April 2026 **Revised: May 2026** **Accepted: July 2026**
DOI: 10.22068/ijmse.4548

Abstract: *This study deals with the dependence of mineral, microstructural, and textural properties on the duration of the indispensable yet easily controlled step of aging. For this purpose, a set of Cu/Zn/Al precursors was synthesized using a conventional constant-pH method. The precipitates were aged for three different durations of zero, two, and four hours. The obtained precipitates, after several washing cycles and overnight drying, were then calcined at 623 K. Precursor and calcined samples were studied in terms of elemental composition, mineral composition, microstructure, texture, porosity, and metallic copper surface area. The results suggest that the dependence of precursor surface area on aging is realized by its dependence on phase composition. In the precipitate aged for two hours, the relative dominance of malachite leads to the highest pre-calcination surface area of 57 m^2/g. The individual thermal behaviors of the precursor phases and their pre-calcination surface area values seem to conjointly determine the post-calcination surface area of the samples. Such that a combination of ripened particle structure and susceptibility to calcination-induced surface deterioration yields the lowest post-calcination surface area after aging for four hours. The calcines derived from the unaged and the two-hour-aged precursors yield surface area values of approximately 57–58 m^2/g, sensibly higher than that of the four-hour-aged sample. The Cu^0 surface area values of the samples depend on aging duration through the effect it imparts on the Cu/Zn-interdispersion of the precursor malachite phase. The highest Cu/Zn-interdispersion is achieved in the two-hour-aged sample that finally exhibited a maximum Cu^0 surface of 112 m^2/g_{Cu}.*

Keywords: *Cu/Zn/Al based composite, Aging, Microstructure, Co precipitation, Supported metallic copper.*

1. INTRODUCTION

Metallic copper dispersed on a support finds application in a variety of fields including petrochemical processes [1-4], purification and pollutant degradation [5], medical practices [6], and disinfestation [7]. These applications are mostly made possible through the interaction of certain entities with or upon the Cu^0 surface. Therefore, Cu^0 surfaces with higher areas are usually preferred. Co-precipitated Cu/Zn/Al systems—owing to the essence of precipitation-based methods and the chemical nature of the Cu/Zn/Al system—provide suitable substrates upon which a metallic phase of high dispersion and tailored properties can be formed.

The effective utilization of a Cu/Zn/Al-based system requires a constant and extensive effort aimed at optimizing its properties. Such an end cannot be met unless a deep understanding of the synthesis method and its effects on the properties of the material at various stages of processing is acquired [8]. The phase composition, microstructure, and textural properties of the precursor to the composite impart significant effects on the overall performance of the final system—which is often closely correlated with metallic copper surface area. The effects of parameters such as pH [1, 9], temperature [1], nature of the starting materials [10, 11], composition [12], aging conditions [13], etc. on these properties have extensively been studied for CuO/ZnO systems. However, the effects of aging time on the phase composition and surface properties have rarely been investigated for the $CuO/ZnO/Al_2O_3$ system. Aging the liquor alters the properties of the precipitates by various mechanisms. Ostwald Ripening—the coarsening of large particles by dissolution and deposition of smaller particles—leads to grain growth and increases the average primary particle sizes of the precipitates [14]. During aging, depending on the aging conditions, crystallization of the amorphous precipitate and transformations between phases of different crystal structures and chemical compositions may also occur. Depending on the application for which the system

is developed, a certain phase or a set of multiple phases may be desired. Co-precipitation of copper and zinc compounds may lead to the formation of various phases of different structures and stoichiometries such as simple carbonates, hydrozincite ($Zn_5(OH)_6(CO_3)_2$), rosasite ($(Cu,Zn)_2(OH)_2CO_3$)), (zincian) malachite ($Cu_2(OH)_2CO_3$), and aurichalcite ($(Cu,Zn)_5(OH)_6(CO_3)_2$). In the case of ternary Cu/Zn/Al systems, the formation of a hydrotalcite-like phase—usually with the formula $(Cu_{0.4}Zn_{0.6})_6Al_2(OH)_{16}CO_3$—may also be promoted [15]. Malachite has often been identified as the desired phase that usually yields high metallic copper surface areas [13]. Other phases, such as aurichalcite, have also been occasionally found to be suitable precursors [16]. Adjusting the aging period is a simple strategy to control the final configuration of the phases composing the system. In the literature, there are a good number of studies that report the separate effects of aging on the mineral composition, microstructure, and texture of these systems. However, there seems to be a lack of focus on the cumulative dependence of these parameters on aging and the interplay between them.

In this study, a set of Cu/Zn/Al precursors was co-precipitated with different aging times. The effects of aging time on properties such as phase composition, microstructure, surface area, pore structure, and metallic copper surface area were investigated, and mechanisms were proposed as to how these effects are realized. These effects were studied not only in terms of how aging modifies the system, but also in terms of certain dependences of the response properties on each other.

2. EXPERIMENTAL PROCEDURES

2.1. Materials

All metal nitrate solutions were prepared industrially by leaching relevant metallic or oxidic raw materials. For this purpose, high-purity metallic copper, ZnO powder, and aluminum ingots were used. Concentrated metal nitrate solutions were diluted to match the desired concentration for synthesis. Industrial-grade sodium carbonate powder was used to prepare the precipitant solution. Distilled water was used in all the steps involved, including the preparation of solutions, washing, etc. Industrial-grade nitric acid was used to adjust the pH of the metal nitrate solutions.

2.2. Sample Preparation

The samples were synthesized by a constant pH co-precipitation method. First, a mixed metal nitrate solution (1 M, 260 ml, pH= 1.5) with the molar Cu:Zn:Al ratio of 54:32:14 and a Na_2CO_3 solution (1 M) were prepared. Then, the metal and alkali solutions were diluted and heated at a constant temperature of 343 K. The injection rate of the metal solution was kept constant, while the injection rate of the alkali solution was carefully manipulated during the precipitation step. This step was followed by aging the liquor at the same temperature. The pH of the liquor was not controlled during the aging step. The liquor was sampled three times at two-hour intervals, yielding an unaged sample and two samples aged for two and four hours. The aged precipitates were filtered and washed several times to ensure that the sodium concentration did not exceed 0.1 wt.%. The washed precipitates were dried at 379 K for about 24 hours and then calcined at 623 K for three hours (with a ramp of three hours). The samples were designated according to Tab. 1.

Table 1. Designation of samples

Sample code	Aging duration (h)
DH_0*	0
DH_2	2
DH_4	4
CH_0	0
CH_2	2
CH_4	4

*The codes starting with the letter D correspond to dry precursors while the codes starting with the letter C represent the calcined samples.

2.3. Characterization

X-ray diffractograms were recorded on a Bruker D8 diffractometer using Cu Kα radiation. The phase identification of the samples was carried out according to the Crystallography Open Database (COD) reference patterns. The adsorption isotherms were obtained by N_2 physisorption using a Micromeritics TriStar II Plus device. The surface areas of the samples were calculated according to the BET (Brunauer–Emmett–Teller) model, and their pore size distributions were determined using the BJH (Barrett-Joyner-Halenda) method. Elemental compositions of the samples were determined by atomic absorption spectroscopy (AAS) with a Varian 240FS spectrometer. A Microtrac BELCAT II analyzer was utilized to carry out reactive frontal chromatography (RFC) for metallic copper surface area evaluation. N_2O was used as the titrant gas on whose chemisorption the RFC measurements were

based. Before RFC measurements, samples were reduced for one hour under the flow of a 5% H_2/Ar gas mixture. SEM (scanning electron microscopy) micrographs were recorded on a TESCAN Mira 2 electron microscope with an accelerating voltage of 15 kV. The thermal decomposition behavior of the samples was studied using differential thermal analysis (DTA) and thermogravimetry (TG) with a Bahr STA 504 device.

3. RESULTS AND DISCUSSION

3.1. Mineral Evolution and Structural Analysis

Fig. 1 a presents the XRD patterns of the DH_0, DH_2, and DH_4 samples. Both hydrotalcite (COD: 96-900-9273) and malachite (COD: 96-500-0044) phases are recognized in the patterns. Almost all peaks of these two phases are present in the diffractograms. However, in the unaged samples, some peaks are identified not as much easily; such that some apparently single peaks are in fact the superimpositions of a number of peaks. This is particularly evident in the peak set located in the range of 2θ= 22.5–25°. In the XRD pattern of the DH_0 sample, it seems as if there is only one peak in that range. By increasing the aging time up to two hours (DH_2), a shoulder appears to the left of the main peak. The main peak in that range corresponds to malachite and the shoulder to hydrotalcite. After another two hours, when the aging duration reaches four hours (DH_4), the two overlapping peaks become almost completely separated. Although peak shift could have possibly contributed to the separation of the two peaks, the main contributor is probably a phenomenon whose nature is closer to crystallinity increase and structural rearrangement. Ostwald ripening and other phenomena of similar nature could also have played parts [14, 17].

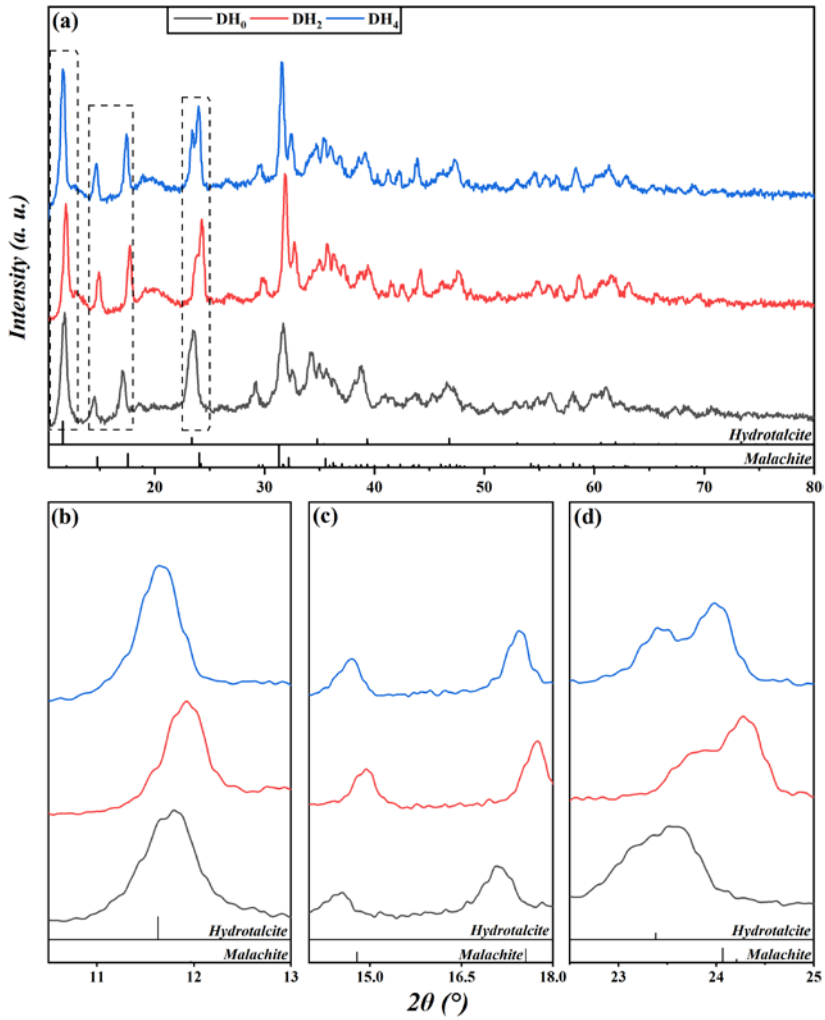

Fig. 1. a) The x-ray diffraction patterns of the precursor precipitates aged for zero (DH_0), two (DH_2), and four (DH_4) hours; magnifications of patterns in ranges of b) 10.5–13°, c) 14–18°, and d) 22.5–25°

The peak shifts observed in the patterns also provide information as to how aging alters the precipitate. In all three of the precursors, the main peak and some of the major peaks of the malachite phase lie at angles higher than those corresponding to pure, zinc-free malachite. This usually follows the incorporation of zinc cations into the malachite structure [18, 19]. The extent of this peak shift depends on the aging time—which is evident in the XRD patterns of both phases. The first two hours of aging have driven the peaks towards higher angles. However, the second two hours of aging have brought back the peaks to angles lower than those observed in the DH_2 samples.

Although all peaks have been shifted in the same direction in each sample, a multitude of mechanisms have probably been at work. Taking into consideration the magnitude of peak shifts (sometimes as great as 1°), it is not wise to bring forth the matters of structural relaxation and lattice stress relief. The main contributor to the peak shifts seems to be the exchange of Zn^{2+} between the phases [17]. During the first two hours of aging, the hydrotalcite phase becomes partially depleted of Zn. This, in turn, leads to a decrease in the d-spacing of some planes and pushes the peaks towards higher angles (Fig. 1 a, b, and c). The malachite phase stands at the receiving end of this exchange; it absorbs the zinc cations, leaving the hydrotalcite structure. The occurrence of such an exchange is in accord with the upward shift of malachite peaks; the incorporation of zinc into the malachite structure reduces the d-spacing of planes by qualifying the Jahn-Teller distortion [14]. In turn, this decrease in the d-spacings translates into peak shifts towards higher angles. However, further aging of the precipitate after two hours imposes a reversal upon the described mechanism, i.e., the hydrotalcite phase becomes richer in zinc while the malachite phase is depleted of it.

The variations in the relative intensities of the two phases might also provide hints as to how the mineral composition of the precipitate is dependent on the aging duration. In the unaged sample, the highest intensity is exhibited by the main hydrotalcite peak. It is not wise to discuss the amounts of phases solely based on XRD patterns. It is, however, clearly evident how effectively aluminum can increase the tendency of the system towards hydrotalcite formation; such that its presence in a small amount has led to the emergence of intense hydrotalcite peaks [2]. Assuming that the amount of a phase is the only factor affecting its peak intensities, the variations in the intensities of the peaks suggest that during the first two hours of aging, the formation of malachite is promoted. Baltes et al. [1] have reported similar results; however, it seems that the over-aging of the precipitate (during the second two hours) favors the formation of hydrotalcite, and the amount of malachite is reduced.

The XRD patterns of the calcined samples are presented in Fig. 2. The characteristic peaks of tenorite (COD: 96-101-1149) are recognizable. Given the very low signal/noise ratios of the patterns, the possible presence of phases other than tenorite cannot be refuted. Zincite (COD: 96-101-1259) is most likely present in the calcined samples. Its main peak, typically lying at about 36.5° is present here as a shoulder to the right of the malachite peak located at 35.6°. The slight shoulder to the low-angle side of the said malachite peak is probably the mark of another major zincite peak. Despite the low calcination temperature, the presence of $ZnAl_2O_4$ spinel, gahnite (COD: 96-101-1002), is also possible. Its major peaks lie close to the main peaks of tenorite and zincite; therefore, a reliable assessment of its presence in the crystalline form requires more than a set of XRD patterns. However, there are pieces of evidence pointing to its possible formation as a mixed Zn-Al oxide.

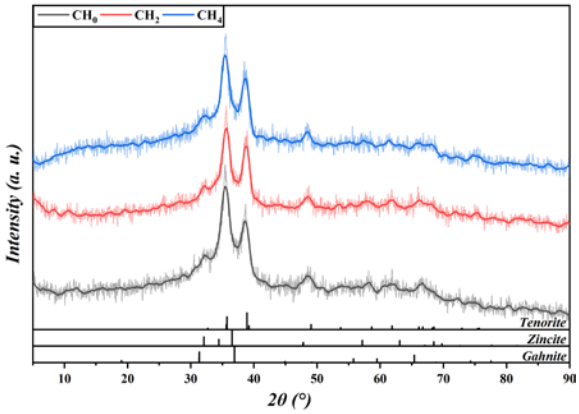

Fig. 2. The x-ray diffraction patterns of the calcined oxidic composites whose precursor precipitates were aged for zero (DH_0), two (DH_2), and four (DH_4) hours

First, the presence of a mixed hydroxycarbonate phase based on aluminum, zinc, and, less likely, copper reduces the dependence of gahnite formation on the heat-induced phenomenon of long-range diffusion, thus partially eliminating the need for high calcination temperatures. Second, the obscurity of the zincite peaks is most probably an outcome

of its reduced amount. Here, the most probable case in which zinc is retained in a phase other than zincite is the formation of a zinc-containing oxidic phase other than zincite. Porta et al. [20] have reported the formation of a highly crystalline gahnite phase after calcination for a prolonged period at 300°C. Therefore, one could assume that calcination at the higher temperature of 350°C for a shorter period could still lead to the formation of an Al-Zn-based spinel-like phase—though not of as much crystallinity and extension.

3.2. Microstructural Analysis

Fig. 3 shows the SEM images of the precursors. Three classes of crystals and crystallites could be distinguished based on size and general morphology. The first class comprises large plate-like crystals of hexagon-like geometries. The second class is composed of elongated rod-like crystallites with polygonal cross-sections. Finally, the last class constitutes very fine crystallites of smaller dimensions and more irregularity. There is not much consensus on the dominant morphology of malachite crystallites; a spectrum of morphologies—including sheet-like and rod-like—has been assigned to malachite [13]. Regarding hydrotalcite, there is no such disparity; such that growth in plate-like morphologies is considered to be a characteristic of hydrotalcite-like phases [21]. Based on this introduction and what will be presented later, the large plate-like crystals are assigned to hydrotalcite and the other two classes to malachite. In the DH_0 sample, all of the three classes can be observed. However, the crystallites of the last class (those of small size and irregular shapes) appear to be larger in this sample than their counterparts in the aged samples. In the DH_2 sample also, the large hexagonal crystals of hydrotalcite and fine irregular crystallites of malachite can be observed (Fig. 3 c and d). The elongated rod-like malachite crystallites are also all recognizable. In the DH_4 sample, hydrotalcite plates seem to have become larger and the irregular malachite crystallites less abundant. The rod-like malachite crystallites—although seemingly in smaller amounts—are still present (Fig. 3e and f). The increase in the intensity of the main hydrotalcite peak during the second two hours of aging was mentioned before. Hydrotalcite crystal growth—also evidenced by the SEM images—could be a major contributor to the intensity increase. In other words, the changes observed in the XRD patterns do not necessarily stem from changes in the amounts of the phases.

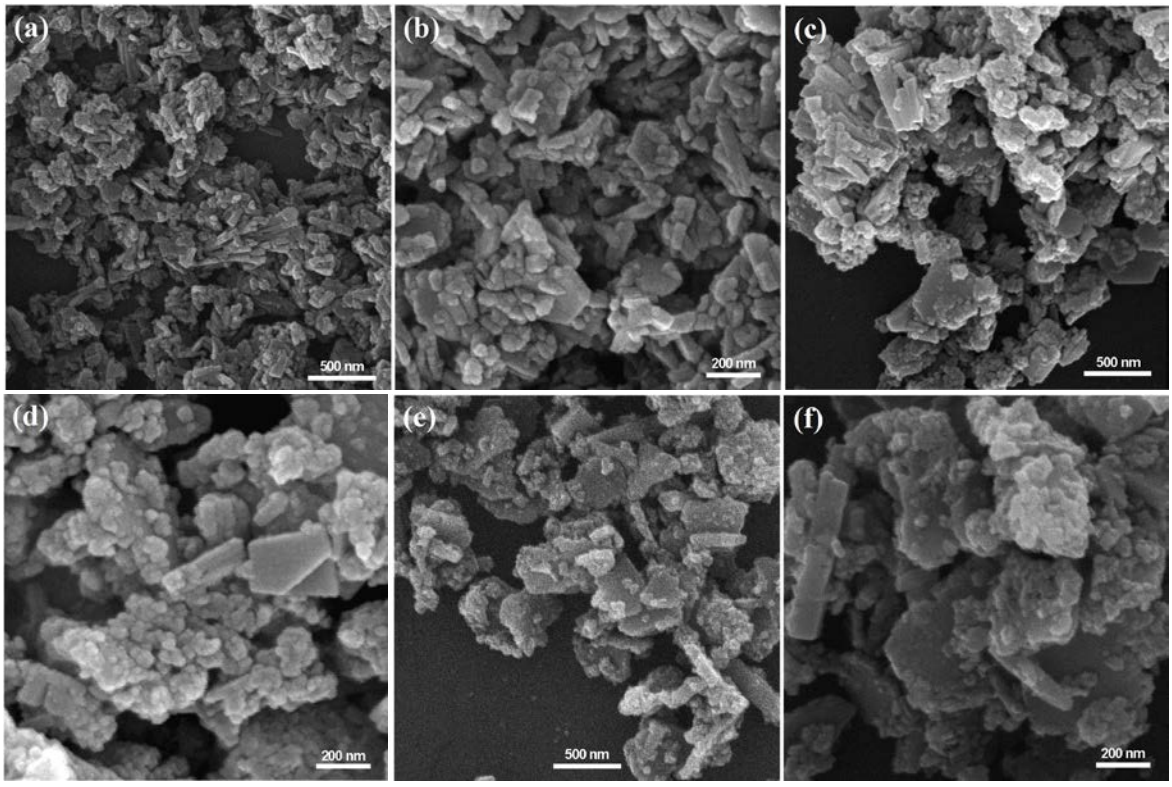

Fig. 3. The FE-SEM micrographs of the precursors aged for (a and b) zero, (c and d) two, and (e and f) four hours at magnifications of 75000x and 150000x

Probably, these changes are partially the result of modifications in the sizes of crystals and crystallites. In the case of malachite, intensity changes in the XRD patterns cannot always be correlated with changes in the texture of the phase. Firstly, this is because malachite crystallites are fine and their scrutiny is difficult. Secondly, as pointed out before, the malachite phase has crystallized in two distinct morphologies, i.e., the XRD patterns arise from two morphologically different sets of crystallites with the same crystal structure. Despite these obstacles, the decrease in the number of irregular malachite crystallites when transitioning from DH_2 to DH_4 is obvious; therefore, the decrease in the intensity of the main malachite peak could be attributed to the reduction in its amount.

Still remains the question of why two sets of crystallites were assigned to malachite. This interpretation of the SEM images might seem a little careless; however, in the case of malachite, it is not very far-fetched. Not only does malachite crystallization in a spectrum of morphologies have precedence, but also its crystallite morphology takes considerable effect from the amount of zinc it hosts [22]. During precipitation, given that zinc incorporation into a copper-based structure proceeds gradually after an initial copper-based precipitate is formed [9, 22], variation in the zinc contents of individual crystallites seems very probable. This probability arises from two assumptions. First, during co-precipitation, the exposure of the solid to the synthesis liquor determines the extent to which the copper-based solid interacts with zinc. Second, because the co-precipitation step is carried out gradually, there are hardly any two portions of precipitate that have been exposed to the liquor for equal periods of time. Probably, when the amount of zinc in crystallite exceeds or falls short of a certain limit, its crystal growth habits change [22]. This chain of causes and effects is probably the root of this diversity in the morphologies of malachite crystallites.

The SEM images of the calcined samples are presented in Fig. 4. Some aspects of these micrographs are of great importance. At lower magnifications, barely any distinctions can be made between the calcined sample and its precursor. Such that, after calcination, features similar to hydrotalcite plates and malachite crystallites are still visible. However, at higher magnifications, crystallites formerly assigned to malachite appear to have been made up of much smaller constituents that are most probably crystallites of zincite and tenorite (Fig. 4b, e, f, and h) that have separated upon calcination. However, it seems that hydrotalcite crystals have not undergone any transformations of this sort. As can be seen in (Fig. 4b, e, and h), the surfaces of these crystals are often smooth. Occasionally, isolated bumps are observed on these plate-like crystals that are probably the decomposition products of the fine malachite crystallites. This is another piece of evidence that supports the idea that these large plate-like features are crystals of hydrotalcite whose complete decomposition is realized at a temperature higher than that of malachite [23]. This is further evidence that zinc is probably present in the samples in forms other than zincite. The possible presence of an Al-Zn-based mixed oxide along with the presence of partially undecomposed hydrotalcite adds to the mentioned obscurity of zincite XRD peaks.

3.3. Surface Area and Porosity Analysis

Adsorption-desorption isotherms, pore size distribution curves, and relevant pore structure parameters of the DH_0, DH_2, and DH_4 samples are presented in Fig. 5. The general geometries of the three isotherms are not much different. As seen in the SEM images, this is also probably evidence that the textures of the three samples are not substantially different. The presence of hysteresis loops in the isotherms suggests the presence of meso-pores in the samples. This is in accord with the average pore sizes of the samples plotted in Fig. 5c. The geometries of the hysteresis loops exhibit similarities to both H3 and H4 hysteresis types. Knowing that the emergence of these two types arises from the presence of sheet-shaped and wedge-shaped pores, respectively, one could assume that the samples contain both these types of pores [24]. It was observed that hydrotalcite crystallizes in the form of large plates and malachite in the form of rod-like and fine irregular crystallites. According to Waller et al. [13], malachite, except after very long aging periods, tends to crystallize in sheet-like morphologies. Therefore, the fine irregular crystallites assigned to malachite are most probably small flakes. In such a system—composed mostly of plate-like and edged features—the presence of sheet-like and wedge-shaped pores is very probable [24].

Fig. 5 c shows the changes in the BET surface areas of the samples. Aging the precipitate for two hours has increased the BET surface area value from 47 to 57 m^2/g. By further aging the precipitate up to four hours, the BET surface area has been

decreased to 49 m^2/g. Similar trends—although not as significant—can be observed for total pore volume and average pore diameter.

As discussed before, the relative intensities of malachite and hydrotalcite change during the aging period. In the DH_0 sample, the main hydrotalcite peak exhibits the highest intensity. In the sample aged for two hours (DH_2), the most intense peak of the XRD pattern is assigned to the malachite phase. After another two hours of aging (DH_4), the relative intensities of the main peaks of the two phases appear to be almost equal. This obvious yet mild fluctuation of peak intensities—only if caused by changes in the amounts of the two phases—is in line with the changes observed in the specific surface areas of the samples. Therefore, the surface area increase observed when transitioning from DH_0 to DH_2 is probably caused by the increase in the amount of malachite (or the decrease in the amount of hydrotalcite). Similarly, the surface area decrease in the second two hours of aging (DH_2 to DH_4) is probably the result of the increase in the amount of hydrotalcite (or the decrease in the amount of malachite). The SEM micrographs also support the presence of such a trend. During the first two hours of aging, the fine malachite crystallites appear to grow in number, leading to an increase in surface area.

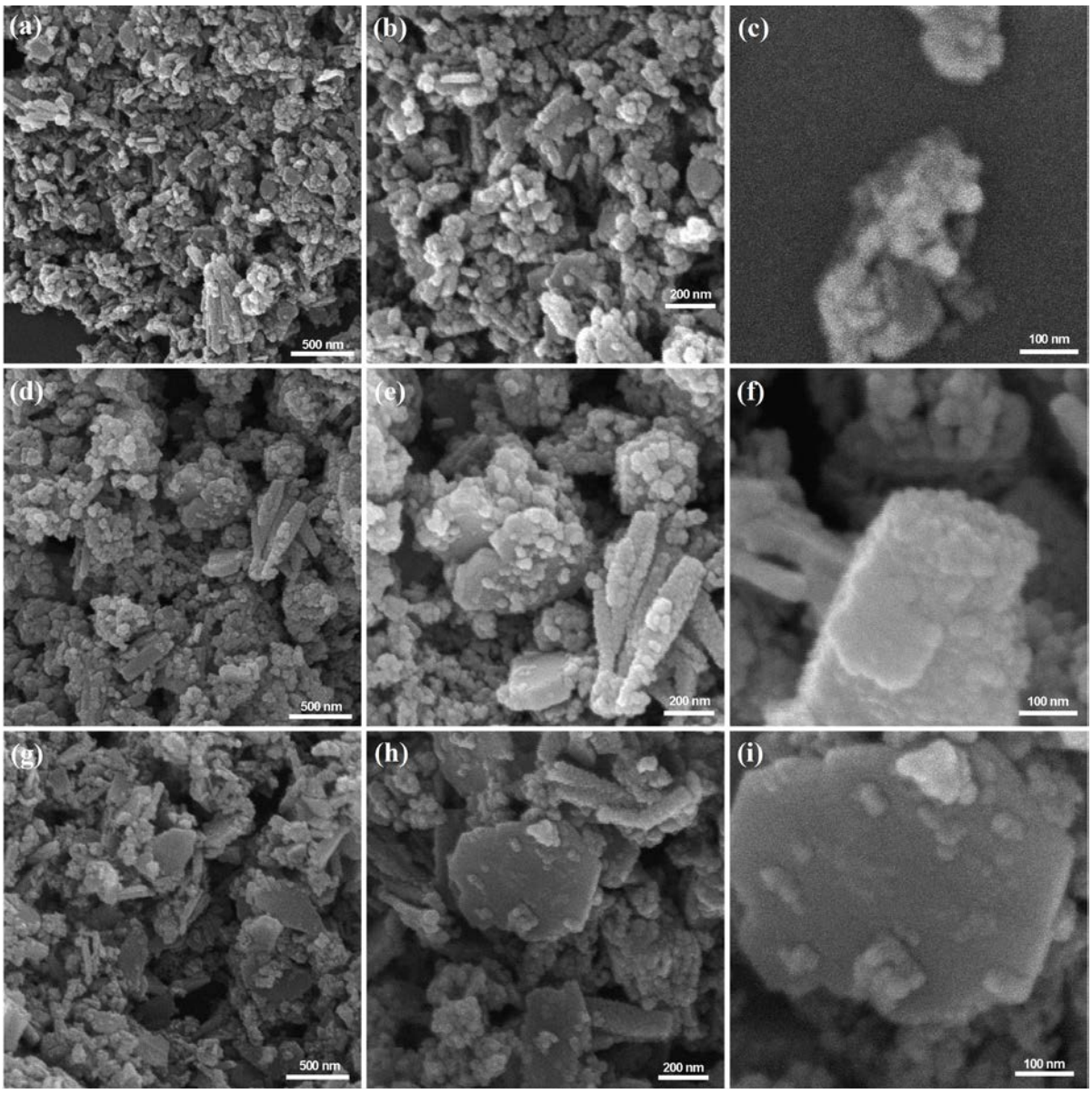

Fig. 4. The FE-SEM micrographs of the calcined oxidic composites whose precursors were aged for (a, b, and c) zero, (d, e, and f) two, and (g, h, and i) four hours at magnifications of 75000x, 150000x, and 350000x

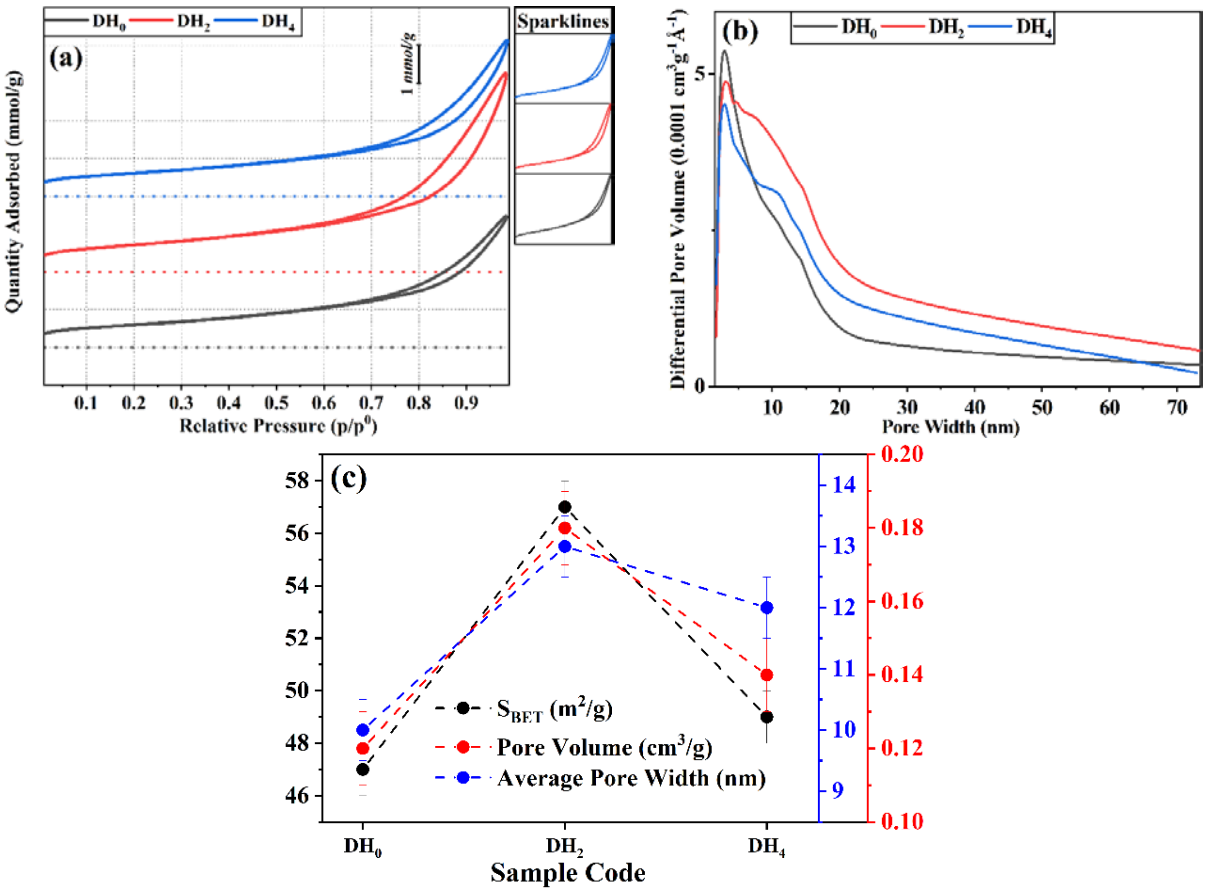

Fig. 5. N_2 physisorption isotherm (a), pore size distribution curve (b), and relevant pore structure parameters (c) of precursor precipitates aged for zero (DH_0), two (DH_2), and four (DH_4) hours. For each adsorption-desorption curve, the dotted lines represent the reference line corresponding to 0 mmol/g of adsorbed N_2

Whether this increase is the result of the transformation of hydrotalcite to malachite or the morphological transformation of malachite (in favor of crystallite refinement) is unknown.

It is relatively evident that the intensity and extent of the role of crystallite growth and refinement have not been constant during the various stages of aging. This is partially because the surface area values of the DH_0 and DH_4 samples are quite close, while the differences in the relative intensities of main malachite and hydrotalcite XRD peaks in these two samples differ sensibly. In other words, during the second two hours of aging, the precursor has undergone a surface area decrease greater than expected.

During the first two hours of aging, the increase in the amount of fine irregular malachite crystallites has led to a surface area increase overcoming the growth of hydrotalcite plates and any other sort of transformation favoring lower surface area. On the other hand, during the second two hours, there are almost no competing factors, and most of the material transformations of the system serve to reduce the surface area. Among these transformations, crystal growth and hydrotalcite formation were treated earlier. The third factor that possibly promotes surface retardation is the morphological change of malachite crystallites. According to Waller et. al [22], after long periods of aging, malachite tends to be present in the form of low-aspect-ratio morphologies rather than sheet-like geometries. Given that crystallites of low aspect ratios (for a given size) provide smaller numbers of surface atoms per volume, they tend to yield lower surface area values. In the present study, such a claim cannot reliably be validated; however, it is fairly obvious that the second two hours of aging have lowered the abundance of fine malachite crystallites. It is a matter of question whether this decrease is the result of malachite-to-hydrotalcite transformation or the morphological transformation of malachite crystallites.

The described reciprocating trend also holds for the BJH curves of the samples; such that at the

end of the fourth hour of aging, the pore size distribution becomes fairly similar to what was observed in the unaged precursor. In all three of the samples, an overpopulation of pores is observed with the approximate average width of 3 nm. Obvious elevations in slope are also observed at pore widths of approximately 8, 11, and 14 nm. These slope changes cannot readily be assigned to pore sets; however, they can be considered relatively populated distribution nodes. The relative broadness of the pore size distributions probably stems from the mineral diversity and the variation of the agglomeration behavior of the system. The 3-nm-wide pores are probably the empty spaces in the agglomerates (or between the primary particles) of the precursor. The sizes of the inter-agglomerate pores are probably scattered across a wider range. It should be carefully noted that although the first two hours of aging do not change the general geometries of the BJH curves considerably, alters certain details of them meaningfully. The alterations imposed during the second two hours are equally intense but do not continue those observed in the first two hours. In fact, it looks as if the second two hours of aging take the precipitate to its unaged form. This is in accord with what was observed in the cases of surface area, phase composition, and microstructure.

Adsorption-desorption isotherms, pore size distribution curves, and some relevant pore structure parameters of the CH_0, CH_2, and CH_4 samples are presented in Fig. 6. After calcination, the general shapes of the isotherms have undergone little change, and the similarities between the precursor isotherms have been preserved [18, 25]. However, the alterations in the BJH curves of samples suggest certain changes in pore structure. The pore size distributions of the precursors—although not especially narrow—exhibit intense overpopulations at approximately 3 nm. In those of the calcined samples, such overpopulations are observed at widths of 3 and 14 nm. The narrower set of pores is probably the remnants of the singular pore set (at 3 nm) observed in the BJH curves of the precursor samples. The wider set of pores—which are also greater in number—has probably emerged following calcination. Interestingly, this second set is recognizable in all three of the calcined samples. This probably means that the same mechanism in the three samples has led to pore-structural transformation.

To further understand the nature of the changes in pore structure, one could compare the total- and micro-pore volumes of the samples and their variations. In all three of the samples, calcination increases the total pore volumes of the samples by a value of approximately 0.1 cm^3/g while the highest micro-pore volume achieved in the samples (before and after calcination) does not exceed 0.0022 cm^3/g. In other words, even the absolute values of micro-pore volume do not contribute meaningfully to the total pore volume, let alone their slight changes induced by calcination. This might be evidence that the calcination-induced changes in the pore structure of the samples are primarily caused by particle rearrangements on an ultra-atomic level. This means that the increase in the total pore volume of the samples is the outcome of expansion-induced pore widening rather than the formation of new pores. The SEM images of the calcined samples also support the validity of such a scenario. As pointed out before, at moderate magnifications, one can hardly notice the effect of calcination on the samples. The oxidic crystallites emerged from decomposition form assemblies of such compactness that the overall shapes of the former precursor crystallites are preserved. Based on these speculations, probably the main aspects of pore-structural transformation are the increase in the distancing of the primary particles and the subsequent expansion of agglomerates.

To address the differences in the calcination behaviors of the precipitates aged for different periods of time, two main factors have to be considered. First is the surface area of the precursor. It is only natural to assume that among a set of precursors that are similar in all aspects except for their surface area values, the one with the highest surface area yields the highest post-calcination surface area. Given the textural character of hydrotalcite compared to that of malachite, precursors based on hydrotalcite rather than malachite exhibit lower pre-calcination surface area values [23]. Second is the difference in the individual behaviors of the two constituting phases—malachite and hydrotalcite—during calcination. The complete decomposition temperature of the hydrotalcite phase (>400°C) lies above the complete decomposition temperature of malachite (≈330°C) [23]. Considering the calcination temperature of the samples (350°C), this suggests that a system composed chiefly of hydrotalcite is less prone to surface deterioration than a system composed chiefly of malachite. Therefore, the susceptibility of a system to calcination-induced surface area deterioration increases as its malachite content increases.

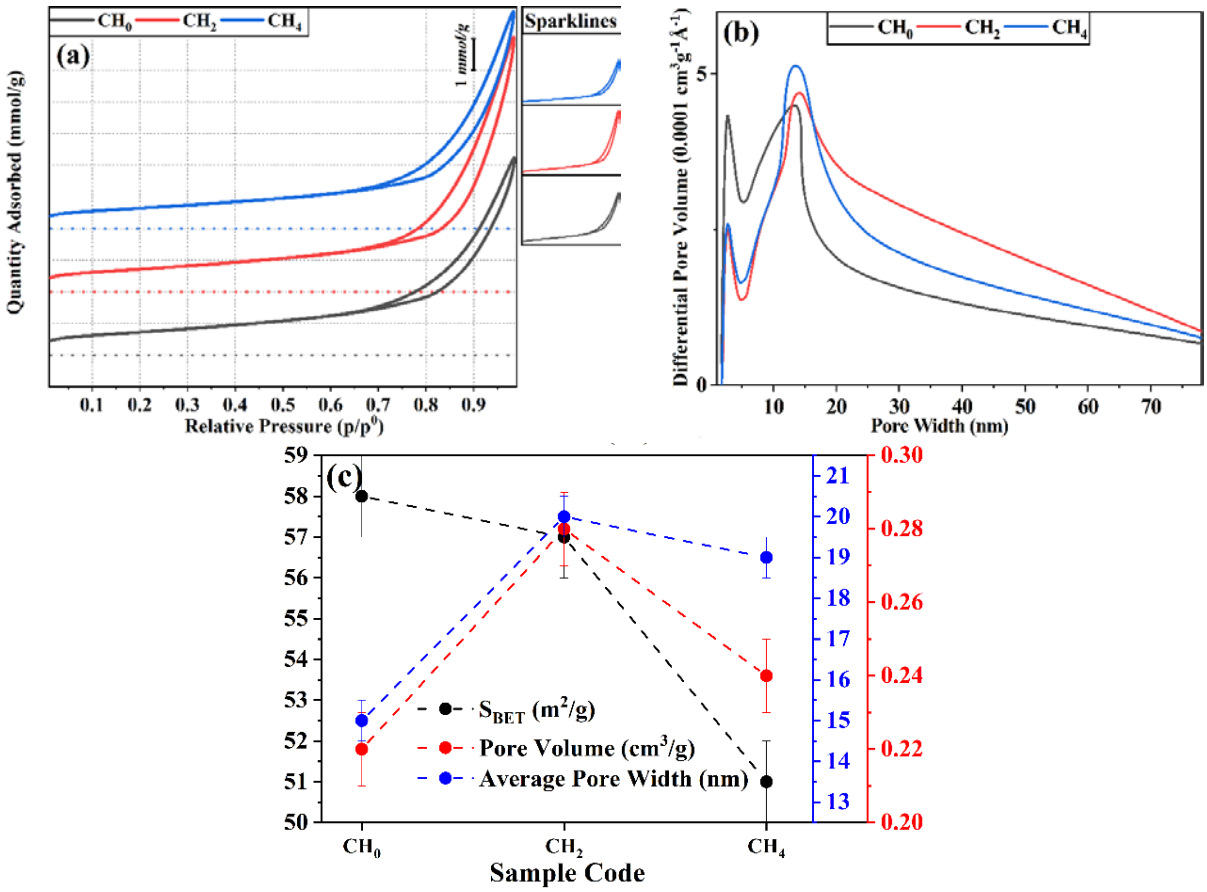

Fig. 6. N_2 physisorption isotherm (a), pore size distribution curve (b), and relevant pore structure parameters (c) of the calcined samples whose precursor precipitates were aged for zero (CH_0), two (CH_2), and four (CH_4) hours. For each adsorption-desorption curve, the dotted lines represent the reference line corresponding to 0 mmol/g of adsorbed N_2

As pointed out before, with the data at hand, one cannot discuss the amounts of phases confidently. But it seems that the DH_0 sample, compared to the rest of the samples, has a slightly higher hydrotalcite/malachite ratio, and this is probably why it has experienced a surface area increase upon calcination. In the other two samples, the effect of hydrotalcite seems to have been moderated by the susceptibility of malachite to calcination, rendering the surface area, all in all, indifferent to calcination. With all this, the CH_2 sample, owing to the high surface area of its precursor, exhibits a surface area value close to that of the CH_0 sample.

3.4. Precursor Thermal Decomposition Behavior

Sample D_2 was selected for further investigation in terms of thermal decomposition behavior. Fig. 7 shows the DTA and TG curves of the sample. The DTA curve presents two major endothermic troughs lying at 159 and 377°C. There also exists a minor endothermic trough lying at approximately 313°C. The trough lying at 159°C is most probably caused by the departure of carbonate groups from the hydrotalcite-like structure. Regarding hydrotalcite-like phases, the literature reports extensive carbonate loss in the temperature range of 100–400°C. However, the volatilization of carbonate seems to be more intense at temperatures close to 150°C. The hydrotalcite-like phase also contains another group of carbonate and hydroxyl species whose departure seems to have been delayed until a temperature as high as 313°C is reached [23].

The trough at 377°C seems to be the result of the simultaneous volatilization of hydroxyl and carbonate species of the malachite phase. The malachite phase is effectively decomposed at this temperature—although it characteristically often contains another class of volatile species that do not seem to have been reflected in the DTA curve of the sample. The continued mass loss of the sample up to 800°C is evidence that such species do exist in the sample. Quite interestingly, the hydrotalcite-

like structures are also often characterized by a high-temperature hydroxyl group that is typically volatilized at temperatures as high as 500°C. However, this step is not reflected in the DTA curve of the sample while the TG curve continues to proceed downward [23].

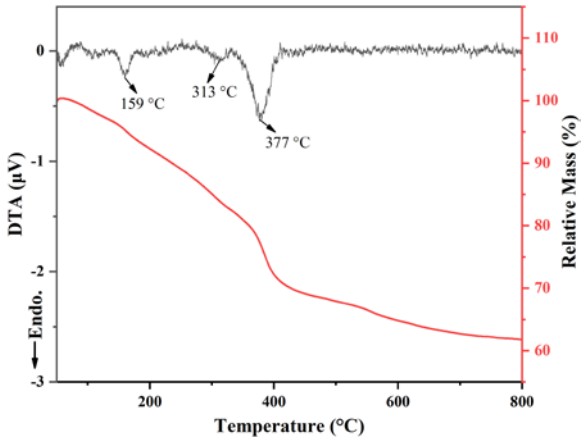

Fig. 7. DTA and TG curves of the precursor sample aged for two hours (D_2)

3.5. Metallic Copper Surface Area

The metallic copper surface area values of the samples take effect from the aging duration slightly but meaningfully. The unaged sample (CH_0) exhibits the lowest Cu^0 surface area (104 m^2/g_{Cu}). Aging the liquor for two hours yields the final metallic-oxidic composite of the highest metallic copper surface area (112 m^2/g_{Cu}). Further aging the liquor for another two hours (in the CH_4 sample), the metallic copper surface area drops to the approximate value of 107 m^2/g_{Cu}. Given the insubstantiality of Cu^0 surface area changes, it is not safe to establish a correlation with CuO crystallite sizes. However, the reciprocating behavior of the parameters treated earlier is observed in the metallic copper surface area too. From this viewpoint, there is an obvious correlation between the zinc content of the malachite phase and metallic copper surface area. It was pointed out earlier that the greater the shift of the main malachite peak to higher angles, the more extensive the incorporation of zinc into the malachite structure. It was also demonstrated that during the first two hours, the main malachite peak goes through an upward shift while the second two hours impose a shift towards lower angles. This trend, agreeing well with that of metallic copper surface area, suggests the dependence of Cu^0 surface area on zinc incorporation into malachite.

The surface area of the metallic phase is affected by several factors. The cationic interdispersion of the precursor is probably the most important material factor [9, 26]. Assuming that the malachite phase is the only contributor to the copper content of the precursor precipitate, for a set of samples of a given copper content, the zinc content of the malachite phase might be a suitable criterion for Cu-Zn interdispersion. In other words, for a given copper content, the more dilute the system with respect to copper, the finer the tenorite crystallites resulting from calcination. According to the XRD patterns and peak positions, among the three investigated samples, DH_2 probably exhibits the highest malachite zinc content and, in turn, the highest Cu-Zn interdispersion. The high interdispersion of this precursor leads to fine CuO crystallites that, upon reduction, yield fine metallic copper crystallites.

4. CONCLUSIONS

In this study, a set of Cu/Zn/Al-based precursors with three aging durations of zero, two, and four hours was synthesized. Effects of aging duration on the mineral composition, microstructure, and texture of the precursors and their calcined counterparts were investigated with an additional focus on the dependence of properties of the oxidic and metallic-oxidic composite on its precursor. The following are the most important results obtained in the study.

- As the aging duration increases, the size of the hydrotalcite plates seems to increase monotonically. The dependence of malachite crystallite size and morphology on the aging duration is more complex; during the first two hours, irregular malachite crystallites tend to become finer and greater in number; however, the second two hours of aging render them less abundant.
- The highest precursor surface area (57 m^2/g) is obtained in the precipitate aged for two hours. After calcination, the sample aged for four hours provides a surface area value sensibly lower than the other two samples. The post-calcination surface area values of the unaged sample (58 m^2/g) and the sample aged for two hours (57 m^2/g) do not differ significantly.
- There seems to exist a correlation between aging duration, Cu-Zn interdispersion, and metallic copper surface area. Aging for two hours promotes zinc incorporation into the malachite structure, leading to a precursor of high Cu-Zn incorporation that finally yields the metallic

copper-containing composite of the highest Cu^0 surface area (112 m^2/g_{Cu}). The second two hours of aging seem to partially deplete the malachite phase of Zn, which, through reducing the cationic interdispersion of the precursor, imposes a decrease in the Cu^0 surface area of the reduced sample.

REFERENCES

[1] C. Baltes, S. Vukojević, and F. Schüth, "Correlations between synthesis, precursor, and catalyst structure and activity of a large set of $CuO/ZnO/Al_2O_3$ catalysts for methanol synthesis", Journal of Catalysis, vol. 258, no. 2, pp. 334-344, 2008/09/10/ 2008. doi: https://doi.org/10.1016/j.jcat.2008.07.004.

[2] Stefan Kaluza et al., "A Novel Synthesis Route for $Cu/ZnO/Al_2O_3$ Catalysts used in Methanol Synthesis: Combining Continuous Consecutive Precipitation with Continuous Aging of the Precipitate", ChemCatChem, vol. 3, no. 1, pp. 189-199, 2011/01/10 2011. doi: https://doi.org/10.1002/cctc.201000329.

[3] Xiaoning Guo, Caihong Hao, Guoqiang Jin, Huai-Yong Zhu, and Xiang-Yun Guo, "Copper Nanoparticles on Graphene Support: An Efficient Photocatalyst for Coupling of Nitroaromatics in Visible Light", Angewandte Chemie International Edition, vol. 53, no. 7, pp. 1973-1977, 2014/02/10 2014. doi: https://doi.org/10.1002/anie.201309482.

[4] Maryam Mirasgari, Seyed Mehdi Alavi, and Mehran Rezaei, "Effects of partial substitution of Cu by Mn and Co in $LaCu_{0.5}Ni_{0.5}O_3$ catalyst synthesized by mechanochemical method in the total oxidation of methane", Res Chem Intermed, vol. 48, no. 9, pp. 3811-3834, 2022/09/01 2022. doi: https://doi.org/10.1007/s11164-022-04775-w.

[5] Atsuhiro Tanaka, Keiji Hashimoto, and Hiroshi Kominami, "Gold and Copper Nanoparticles Supported on Cerium(IV) Oxide—A Photocatalyst Mineralizing Organic Acids under Red Light Irradiation", Chem CatChem, vol. 3, no. 10, pp. 1619-1623, 2011/10/17 2011. doi: https://doi.org/10.1002/cctc.201100158.

[6] L. Suresh, J. S. Bondili, and P. K. Brahman, "Development of proof of concept for prostate cancer detection: an electrochemical immunosensor based on fullerene-C60 and copper nanoparticles composite film as diagnostic tool", Materials Today Chemistry, vol. 16, p. 100257, 2020/06/01/ 2020. doi: https://doi.org/10.1016/j.mtchem.2020.100257.

[7] Indrani Das Jana, Partha Kumbhakar, Saptarshi Banerjee, Chinmayee Chowde Gowda, Nandita Kedia, Saikat Kumar Kuila, Susanta Banerjee, Narayan Chandra Das, Amit Kumar Das, Indranil Manna, Chandra Sekhar Tiwary, and Arindam Mondal, "Copper Nanoparticle–Graphene Composite-Based Transparent Surface Coating with Antiviral Activity against Influenza Virus", ACS Applied Nano Materials, vol. 4, no. 1, pp. 352-362, 2021/01/22 2021. doi: 10.1021/acsanm.0c02713.

[8] Gerhard Ertl, Helmut Knözinger, Ferdi Schüth, and Jens Weitkamp, Eds. Handbook of Heterogeneous Catalysis. 2nd Edition. Weinheim: Wiley-VCH, 2008, pp. 4270–8 volumes.

[9] J. L. Li and T. Inui, "Characterization of precursors of methanol synthesis catalysts, copper/zinc/aluminum oxides, precipitated at different pHs and temperatures", Applied Catalysis A: General, vol. 137, no. 1, pp. 105-117, 1996/03/28/ 1996. doi: https://doi.org/10.1016/0926-860X(95)00284-7.

[10] G. Sengupta, D.P. Das, M.L. Kundu, S. Dutta, S.K. Roy, R.N. Sahay, K.K. Mishra, "Study of copper—zinc oxide catalysts, characterisation of the coprecipitate and mixed oxide", Applied Catalysis, vol. 55, no. 1, pp. 165-180, 1989/11/01/ 1989. doi: https://doi.org/10.1016/S0166-9834(00)82326-X.

[11] A. M. Pollard, M. S. Spencer, R. G. Thomas, P. A. Williams, J. Holt, and J. R. Jennings, "Georgeite and azurite as precursors in the preparation of co-precipitated copper/zinc oxide catalysts", Applied Catalysis A: General, vol. 85, no. 1, pp. 1-11, 1992/06/04/ 1992. doi: https://doi.org/10.1016/0926-860X(92)80125-V.

[12] Frank S. Stone and David Waller, "Cu–ZnO and $Cu–ZnO/Al_2O_3$ Catalysts for the Reverse Water-Gas Shift Reaction. The Effect of the Cu/Zn Ratio on Precursor Characteristics and on the Activity of the Derived Catalysts", Top. Catal., vol. 22, no. 3, pp. 305-318, 2003/04/01 2003. doi: https://doi.org/10.1023/A:1023592407825.

[13] David Waller, Diane Stirling, Frank S. Stone,

and Michael S. Spencer, "Copper–zinc oxide catalysts. Activity in relation to precursor structure and morphology", Faraday Discussions of the Chemical Society, 10.1039/DC9898700107 vol. 87, no. 0, pp. 107-120, 1989. doi: https://doi.org/10.1039/DC9898700107.

[14] Muhamad Ernee, Ramli Irmawati, Taufiq-Yap Yun Hin, Abdullah A., Kniep B.L., Girgsdies F., and Ressler T., "Comparative study of Cu/ZnO catalysts derived from different precursors as a function of aging", Catalysis Today, vol. 131, no. 1, pp. 118-124, 2008/02/29/ 2008. doi: https://doi.org/10.1016/j.cattod.2007.10.010.

[15] Richard G. Herman, Charles E. Bogdan, Philip L. Kumler, and Deanna M. Nuszkowski, "Preparation and characterization of hydroxycarbonate precursors that yield successful alcohol synthesis catalysts", Materials Chemistry and Physics, vol. 35, no. 3, pp. 233-239, 1993/10/01/ 1993. doi: https://doi.org/10.1016/0254-0584(93)90137-B.

[16] T. Fujitani and J. Nakamura, "The effect of ZnO in methanol synthesis catalysts on Cu dispersion and the specific activity", Catal Lett, vol. 56, no. 2, pp. 119-124, 1998/12/01 1998. doi: https://doi.org/10.1023/A:1019000927366.

[17] Bettina Bems, Michael Schur, Alina Dassenoy, Heinz Junkes, Daniel Herein, and Robert Schlögl, "Relations between Synthesis and Microstructural Properties of Copper/Zinc Hydroxycarbonates", Chemistry–A European Journal, vol. 9, no. 9, pp. 2039-2052, 2003/05/09 2003. doi: https://doi.org/10.1002/chem.200204122.

[18] Malte Behrens, "Meso- and nano-structuring of industrial Cu/ZnO/(Al_2O_3) catalysts", J. Catal., vol. 267, no. 1, pp. 24-29, 2009/10/01/ 2009. doi: https://doi.org/10.1016/j.jcat.2009.07.009.

[19] N. Mota, R. Guil-Lopez, B. G. Pawelec, J. L. G. Fierro, and R. M. Navarro, "Highly active Cu/ZnO–Al catalyst for methanol synthesis: effect of aging on its structure and activity", RSC Advances, 10.1039/C8RA03291B vol. 8, no. 37, pp. 20619-20629, 2018. doi: http://dx.doi.org/10.1039/C8RA03291B.

[20] Porta Piero, Campa Maria Cristina, Fierro Giuseppe, Jacono Mariano Lo, Minelli Giuliano, Moretti Giuliano, Stoppa Luisa, "Cuo–ZnO–Al_2O_3 mixed oxides: preparation, bulk and surface characterization", Journal of Materials Chemistry, 10.1039/JM9930300505 vol. 3, no. 5, pp. 505-511, 1993. doi: http://dx.doi.org/10.1039/JM9930300505.

[21] Malte Behrens, Igor Kasatkin, Stefanie Kühl, and Gisela Weinberg, "Phase-Pure Cu, Zn, Al Hydrotalcite-like Materials as Precursors for Copper-rich Cu/ZnO/Al_2O_3 Catalysts", Chem. Mater., vol. 22, no. 2, pp. 386-397, 2010/01/26 2010. doi: https://doi.org/10.1021/cm9029165.

[22] Huayan Zheng, Nilesh Narkhede, Huacheng Zhang, and Zhong Li, "Oriented Isomorphous Substitution: An Efficient and Alternative Route to Fabricate the Zn Rich Phase Pure $(Cu_{1-x},Zn_x)_2(OH)_2CO_3$ Precursor Catalyst for Methanol Synthesis", ChemCatChem, vol. 12, no. 7, pp. 2040-2049, 2020/04/06 2020. doi: https://doi.org/10.1002/cctc.201902286.

[23] M. J. L. Ginés and C. R. Apesteguía, "Thermal decomposition of Cu-based hydroxycarbonate catalytic precursors for the low-temperature co-shift reaction", Journal of Thermal Analysis, vol. 50, no. 5, pp. 745-756, 1997/12/01 1997. doi: https://doi.org/10.1007/BF01979204.

[24] Thommes Matthias, Kaneko Katsumi, Neimark Alexander V., Olivier James P., Rodriguez-Reinoso Francisco, Rouquerol Jean and Sing Kenneth S.W., "Physisorption of gases, with special reference to the evaluation of surface area and pore size distribution (IUPAC Technical Report)", vol. 87, no. 9-10, pp. 1051-1069, 2015. doi: https://doi.org/10.1515/pac-2014-1117.

[25] Maria Turco, Giovanni Bagnasco, Claudia Cammarano, Pasquale Senese, Umberto Costantino, and Michele Sisani, "Cu/ZnO/Al_2O_3 catalysts for oxidative steam reforming of methanol: The role of Cu and the dispersing oxide matrix", Appl. Catal. B Environ., vol. 77, no. 1, pp. 46-57, 2007/11/30/ 2007. doi: https://doi.org/10.1016/j.apcatb.2007.07.006.

[26] Guo-Cheng Shen, Shin-ichiro Fujita, Susumu Matsumoto, and Nobutsun Takezawa, "Steam reforming of methanol on binary CuZnO catalysts: Effects of preparation condition upon precursors, surface structure and catalytic activity", Journal of Molecular Catalysis A: Chemical, vol. 124, no. 2, pp. 123-136, 1997/10/10/ 1997. doi: https://doi.org/10.1016/S1381-1169(97)00078-2.